Vacuum ultraviolet-absorption spectroscopy and delocalized plasma-induced emission used for the species detection in a down-stream soft-etch plasma reactor

Robert Soriano, Gilles Cunge, Nader Sadeghi

VUV-absorption spectroscopy and delocalized plasma-induced emission used for the species detection in a down-stream soft-etch plasma reactor

Autors

R.Soriano, G.Cunge and N.Sadeghi

Univ. Grenoble-Alpes, CNRS, CEA/LETI Minatech, Laboratoire des Technologies de la Microélectronique, Grenoble, France

Abstract

The VUV-absorption spectroscopy (AS) and the emission spectroscopy (ES) from delocalized probe plasma, are implemented in the downstream chamber of a soft-etch industrial plasma reactor. A CCP plasma, running in the upper compartment in $He/NF_3/NH_3/H_2$ mixtures at about one Torr, produces reactive species which flow through a shower head into a downstream chamber, where they can etch different µ-electronics materials: Si, SiO_2, SiN,... The ES reveals the presence of F and H atoms, while the dissociation rates of NF_3 and NH_3 are deduced from the AS, as well as the density of HF molecules, produced by chemical chain-reactions between dissociation products of NF_3, NH_3 and H_2.

1. Introduction

Downstream etchers known as remote plasma sources (RPS) were introduced in the early 70's for resist stripping applications [1, 2]. However, until recently, they have drawn relatively little scientific interest compared to other plasma sources because they inevitably lead to isotropic etching, which restrict their use to specific applications. But as the size and thickness of transistors continue to shrink, new processes are required to etch high aspect ratio (AR) nano-features. For example, ultrahigh selective isotropic etching in RPS is needed for specific steps involved in the patterning of FinFet [3] transistors and 3D Nand memories [4]. RPS processes have also started to be investigated [5] to replace wet processes that show severe limitation to remove materials in high aspect ratio (AR) structures due to capillary forces. Finally, plasma induced damage (mostly caused by energetic ions and photons) has become a major concern and new etching technologies (involving RPS in combination with typical plasmas) such as the Smart Etch [6] and other ALE processes [7] have been introduced to etch materials anisotropically without damages. As a matter of fact, the interest of RPS lies in their capabilities to produce purely chemical etching with radicals leading to high selectivity and absence of structural damages in underlayers.

In many of the above mentioned applications, the goal is to etch selectively a Si alloy respectively to another Si alloy (e.g. Si, SiN and SiO_2), which can be achieved in F-based RPS plasmas. NF_3 is typically used as F source due to its high cross section for dissociative electron attachment [8]. Further, F atoms density in the discharge can be controlled by adding H or O containing gases into NF_3. For example, downstream plasmas in NF_3/O_2 mixtures have been used to etch selectively SiN to SiO_2 [9], and remarkable performances were obtained recently [4] to remove SiN from trenches with AR of 100, thus performing better than in wet processes.

On the other hand, H addition to NF_3 in RPS leads to new etching possibilities. Initially, such processes were introduced [10] to deoxidize silicon surfaces, i.e. etch SiO_2 selectively to Si prior to epitaxy, or to clean STI trenches. These processes were achieved in NF_3/H_2 [11, 12] or NF_3/NH_3 chemistry [13]. The addition of hydrogen to NF_3 does not serves only to reduce F atoms but also promotes the formation of new radicals such as HF or NH_4F, which are believed to be the precursor to the formation of ammonium salts $(NH_4)_2SiF_6$ selectively on SiON and SiOx surface [14, 15, 16]. In this case, there is no direct etching of the surface during the RPS step: the salt forms selectively with material to be etched and must then be sublimated to readily etch the material.

Several innovative Etching processes have been developed recently based on this phenomenon, including the so called Smart Etch process [6] and several Atomic Layer Etching processes [7, 17] all of which are two step processes: the material is first modified anisotropically on a well-controlled depth by a given plasma and the modified layer is then etched selectively in a second step by a RPS in NF_3/H_2 or NF_3/NH_3. The "Smart Etch" process is using energetic H_2 or He ions generated in a CCP plasma for the first step, thus modifying several nm of SiN material by ion implantation (the use of light ions prevents SiN sputtering) [18, 19]. Initially, the modified SiN* layer was removed selectively to pristine SiN by a wet HF [6] or by gaseous HF [20]. But this doesn't allow cycling the two step of the process with a good throughput. By contrast, by removing the modified SiN* layer with an RPS in NF_3/NH_3 mixtures [21]**,** it becomes possible to perform the implantation and RPS steps without air exposure, either on two plasma chambers in the same cluster, or even in the same specifically design chamber [22]**.** For industrial applications, the salt formed during the RPS step can be sublimated either by heating [17], or simply by reducing the pressure before the next implantation step [22]. Recent work [22] has demonstrated that $(NH_4)_2SiF_6$ salt formation is efficient only on oxidized surfaces, explaining the SiO_2/Si and SiO_x/SiN etching selectivity as well as the SiN*/SiN selectivity in the Smart Etch process: even if oxygen free H_2 or He plasma are used to modify the SiN there was actually a considerable amount of O implantation in the SiN* originating from plasma impurities. Interestingly, while the salt formation has been widely analyzed through surface diagnostics, the origin of radicals that are precursors to their formation remains highly speculative; since the gas phase of NH_3/NF_3 and NF_3/H_2 RPS has never been analyzed. The consensual [10, 15, 21, 22, 23, 24] mechanism for the salt formation is the reaction :

$$SiO_2 + 2NH_4F + 4HF \rightarrow (NH_4)^2SiF_6 + 2H_2O \quad (1)$$

Therefore, NH_4F, HF and $NH_4F(HF)$ are typically assumed to be formed in the plasma and hence they react with the surface. This assumption remains speculative even if the work from Ogawa [15] indirectly suggests that NH_4F could be produced from the reaction of NH_3 gas with some fragment of NF_3 (formed by heating NF_3). As a matter of fact, the formation of HF in the plasma can be expected to play a significant role in the overall chemistry and we can expect HF to be formed by the chain reactions (2-4) (well known in HF laser physics) [25, 26, 27, 28, 29, 30]:

$$H_2+F \rightarrow HF+H \quad (2)$$

$H+NF_X$ (x=1,2) → $HF+NF_{x-1}$ (3)

NH_3+F → NH_2+HF (4)

In the present paper, we apply the VUV Broad-Band absorption spectroscopy (BBAS) in the 120-200 nm range [31, 32] with a deuterium lamp as light source for the real time monitoring of etching agents and etch products in the downstream of NF_3-NH_3-H_2 containing plasmas of an AMAT RPS reactor especially designed to perform Smart Etching and described in details in ref [22]. Besides the VUV-BBAS, we also have implemented a probe pulsed DC discharge to follow, by actinometry, the density of F and H atoms in the downstream chamber. By directly measuring the densities of NH_3, NF_3 and HF, as well as the variation of F and H densities as a function of the operating condition, we could get insights into the complex chemistry of these RPS plasmas.

2. Experimental set-up

2.1 Plasma reactor

The experiments are carried out in an industrial 50 cm diameter remote plasma reactor (*frontiers* from Applied Materials) used for the soft etching of 30 cm diameter wafers. It is composed of two chambers separated by an about 50 mm thick shower head. As shown in figure 1, the gas, whose main component is helium and contains a few percent of H_2, NF_3 and NH_3, enters the top compartment, flows through the shower head to expand into the downstream compartment and is then pumped out with a 200 l/s dry primary pump. The total gas flow rate is about 2000 sccm and the gas pressure in the downstream chamber (*DSC*), measured with a capacitance gauge, is maintained to 1 Torr with a throttle valve located on the pumping pipe. A Capacitively Coupled Plasma (*CCP*) is generated in the top compartment with up to 500 W power of 13.56 MHz radiofrequency discharge. Radicals and atoms produced by the discharge are transported by the gas flow into the *DSC* but the plasma production zone is limited by the shower head, blocking the extension of the discharge into the downstream compartment. Thus, only radicals are responsible for the soft etching of the wafer positioned in the *DSC*, without any assistance by ion bombardment, as is the case in usual reactive ion etching processes [33]. Due to the absence of viewports in the *CCP* zone of the reactor, any diagnostic technique can be implemented to characterize the *CCP* plasma. However, atoms and molecules produced by the dissociation of injected molecules in this plasma and transported to the *DSC* have been monitored in this chamber

by the vacuum ultraviolet broad-band absorption spectroscopy (*VUV-BBAS*) and by optical emission spectroscopy (*OES*). But, as a consequence of the absence of energetic electrons in the downstream plasma, any optical radiation is emitted from this region. Thus, to monitor the density of H and F atoms present in the downstream chamber, a small tube (about 4 cm inner diameter, 10 cm long) is connected to the *DSC* through a 4 cm diameter hole on the reactors' wall and an auxiliary plasma (*AP*) is generated inside this tube by applying a positive high voltage (*HV*) to an isolated, 0.2 cm diameter, 3 cm long copper road which penetrate into the tube by one of its end, as shown in figure 1. The opposite end of the tube is sealed by a quartz window for the *OES* and the inner walls of the tube act as a cathode for the auxiliary discharge.

2.2 Actinometry with auxiliary plasma

To follow the variation of H and F atoms densities produced by the *CCP* discharge, the optical emission of the auxiliary discharge is collected by an optical fibre, whose other end is set on the entrance slit of a 50 cm focal length monochromator (Acton 500 i), equipped with a 600 groves/mm grating and backed by a 1024 elements, 25 µm pitch photodiode array. A 112 kΩ resistor, placed in series with the *HV* supplier, limits the peak discharge current of the *AP* to about 8 mA with 1 kV applied voltage. And moreover, the HV is modulated at 120 Hz, with 5% duty cycle to keep as low as possible the dissociation of the gas inside the auxiliary discharge tube. Thus, we assume that the recorded emission intensities from the excited states of H, F and He atoms, at 656.3, 703.7 and 706.5 nm lines, respectively, are proportional to the densities of these atoms in the downstream chamber. The actinometry method [34, 35], with 706.5 nm helium line for the reference intensity, is used to follow changes on H and F atoms' densities when varying the amount of the added gases to helium. We are aware that the large difference between the excitation energies of helium line (22.7 eV) and that of H line (12 eV) and F line (14.7 eV) render questionable the use of helium as actinometer gas [34]. But we consider that with helium remaining the main component of the feed gas, the electron temperature in the auxiliary plasma shouldn't significantly change with the variation of the minor components, which are H_2, NF_3, NH_3 and radicals produced by their dissociation in the CCP plasma. Thus, assuming constant excitation cross-section of species and neglecting the quenching of excited states by the gas, we apply the simplified actinometry equations [35, 36]:

$$I_{706} = G.K_{706}.n_e.[He] \quad (5)$$

$$I_X = G.n_e.(K_X.[X] + K_{PX}.[PM]) \quad (6)$$

Where *G* is a geometric factor, [*He*] and [*X*] (with X=F or H) are the densities of helium and atoms X, with I_{706} and I_X being their respective recorded intensities and [*PM*] is the density of the primary precursor molecule (NF_3, H_2 or NH_3) added to helium whose dissociative excitation in the *AP* can contribute to the recoded intensity I_X and K_i are the respective rate coefficients for the production of X atom in the observed excited state from species "*i*". To write (6), the contribution to the I_X intensity of the other dissociation products of the gas in the CCP, excepted X atoms, is neglected. The excitation coefficient K_{PM} of the precursor molecule is deduced by measuring I_X when known amount of the *PM*, diluted in helium, is introduced into the reactor in the absence of the CCP discharge. And, as will be described in the following section, the density of precursor molecules NF_3 and NH_3 in the downstream chamber, thus in the auxiliary plasma, can be measured by the *VUV-BBAS*. Hence the contribution of *PM* to the I_X can be evaluated and subtracted for obtaining I_X^c, the intensity originated from the sole direct excitation of the ground state X atom in the auxiliary plasma. And finally, the variation of the density of *X* atoms in the downstream chamber, when changing the gas mixture and *CCP* discharge conditions, can be followed by using the simplified equation:

$$[X] \sim [He] \frac{I_X^c}{I_{706}} \quad (7)$$

2.3 Broad-band absorption spectroscopy

The absolute densities of NH_3 and NF_3 molecules in the downstream chamber, thus their dissociation rates in the CCP chamber, as well as the density of HF molecules formed from the dissociation products, have been measured by the broadband absorption technique [37, 38, 39]. A schematic of the top view of the reactor, with the VUV-BBAS set-up is shown in Figure 2. Shortly, the light source is a high-pressure deuterium (D_2) lamp (X2D2 from Hamamatsu) that emits a continuum radiation down to 120 nm. A VUV grade parabolic mirror produces a collimated, 1 cm diameter, light beam at 90° from the incident light. This VUV beam crosses the downstream chamber, through two optical ports facing each other and equipped with MgF_2 windows, at about 5 cm below the shower head (see Fig. 1). At the exit of the second window, another VUV grade parabolic mirror focuses the VUV beam onto the entrance slit of a 20 cm focal length VUV

spectrometer (Jobin-Yvon H20-UVL), equipped with a 1200 groove/mm concave VUV grating. The exit port of the spectrometer was modified to accept a VUV CCD camera (Newton DO940 for X-ray & VUV from Andor) with 2048x512 pixels of 13.5 µm pitch size. In the central part of the CCD (between pixels 600 to 1500), the linear dispersion is 0.047 nm/pixel and the ultimate spectral resolution of the system is about 0.14 nm with 20 µm entrance slit width. But the spectral resolution is degraded in the edges of the CCD. Turbomolecular pumps maintain a background pressure below 10^{-4} Torr in the entire optical path of the VUV light outside the reactor chamber (D_2 lamp to the reactor input window and the exit window to the CCD). As usual in *BBAS* experiments [38], the absorption spectra of the gas in the downstream chamber is obtained by recording three spectra with the CCD: i) the background with the lamp off (*BG*), ii) the emission of the lamp without the gas flow, L_0 and iii) the transmitted light of the lamp ($I_P(\lambda)$) with the gas flow On. Remark that the absence of energetic electrons in the *DSC* results in the absence of plasma emission, which can be neglected. The absorbance spectra (A_λ), which is related to the wavelength dependent absorption cross-section $\sigma(\lambda)$ of the molecules through the Beer-Lambert law, is obtained by:

$$[A]_\lambda = Ln\left(\frac{I_0(\lambda)}{I_T(\lambda)}\right) = Ln\left(\frac{L_0(\lambda)-BG}{I_P(\lambda)-BG}\right) = \sum_i \sigma_i(\lambda).l.N_i \quad (8)$$

where I_0 and I_T are the intensity of the incoming and transmitted VUV light, index "*i*" refers to different absorbing species present in the chamber with density N_i and l is the absorption length. Although the absorption cross-sections of NH_3 [40, 41, 42, 43] and NF_3 [44, 45, 46] have been reported in the literature, for the determination of their partial pressures in the downstream chamber we have used our own collection of absorbance spectra recorded when the reactor was filled with these gases at different known pressures in the absence of discharge. This collection of spectra constitutes some sort of abacus. As an example, recorded absorbance spectra of NH_3 and NF_3 are reported in figures 3 and 4 for a few indicated pressures. This way of proceeding has the advantage of being insensitive to changes on the spectral profile of NH_3 with the spectral resolution of the spectrograph + CCD. Opposite to the NF_3 case, for which the VUV photon absorption ends up in a pre-dissociated continuum, the upper states of the VUV transitions in NH_3 are Rydberg states, with vibrational and rotational levels. In Fig. 3, transitions to these electronic states and corresponding vibrational levels are identified, but the rotational structure cannot be resolved. The absorption profile is thus composed of many narrow ro-vibrational transitions and important

modifications on the behavior of the absorbance curves can be observed with the spectral resolution of the detection system (compare spectra in [41] and [43]). It should be pointed out that the entrance slit of the spectrometer was kept unchanged and consequently, the spectral resolution was identical in all spectra recorded in plasma conditions and for the abacus. Also, using the calibration spectra of the abacus for the determination of NH_3 partial pressure under plasma conditions eliminates a possible error source by saturation of the peak absorbencies [39].

3. Results and discussion

3.1 Characterisation of HF spectrum

Dissociation of NF_3 in CCP plasma produces F atoms that can rapidly react with H containing molecules to form HF molecule [26, 28]. Strong absorption spectra of HF in the VUV spectral range have been reported in the literature [47, 48] and its detection by VUV-BBAS was thus highly expected. The experiments have been carried out in the afterglow of NF_3/H_2 mixture in which HF is produced by the reaction of F atoms resulting from the plasma dissociation of NF_3 with H_2 molecule (reaction (2)), for which a rate coefficient k_2=2-3 x 10^{-17} $m^3.s^{-1}$ has been reported [26, 28]. Absorption spectra recorded in the downstream chamber without and with a discharge in the CCP chamber are shown in figure 5. The experimental steps are:

1) A mixture of 4% NF_3/ 9% H_2 diluted in helium is flown through the reactor and the exit throttle vale is adjusted for obtaining 1 Torr total pressure in the downstream chamber.
2) The recorded VUV spectra is identical to the one obtained at 40 mTorr of NF_3 from the abacus of figure 4. As NF_3 doesn't react with H_2, we conclude that the partial pressure of NF_3 in the *DSC* is 40 mT in the absence of plasma.
3) A 250 W plasma is stuck in the CCP compartment and after a few seconds of stabilisation time, a new VUV absorption spectrum is recorded. As seen in Fig. 5, the shape of this new spectrum is totally different from the previously recorded in the absence of CCP plasma. This modification revels absorption by new species formed under the CCP plasma action, which, as previously discussed, is HF molecule. However, the high wavelength tail of the new spectrum can be fitted by the absorption spectrum of NF_3 at a pressure of 24 mTorr, indicating that about the half of the NF_3 molecules was dissociated by the CCP plasma. The new spectrum, obtained when subtracting the absorption curve

of 24 mTorr NF_3 from the recorded spectra with the plasma ON, corresponds to the $A^1\Pi \leftarrow X^1\Sigma^+$ absorption spectrum of HF molecules. This attribution is justified by the similarity of this spectrum with the one obtained by Nee *et al* from synchrotron radiation absorption by HF gas [47]. These authors also provide the wavelength dependent absorption cross section, from which the absorbance can be converted to the density of HF in the DSC by using Eq. (8). The deduced partial pressure of HF in the example presented in Fig. 5 is 40 mTorr. Given that $A^1\Pi$ state is pre-dissociated, because its energy is above the D°=5.87 eV dissociation limit of HF [49], the HF($A^1\Pi \leftarrow X^1\Sigma^+$) absorption spectrum is a continuum, with its absorbance being scaled with the HF density, for fixed absorption length. We will thus use in the following the absorbance spectrum deduced from NF_3/H_2 plasma, depicted in figure 5, for the determination of the amount of HF molecules produced in other plasma conditions.

As an example, in figure 6 are shown absorption spectra recorded in the downstream chamber without and with CCP plasma in 1.6% NF_3/ 2% NH_3 diluted in helium gas at a total flow rate of 2 l/min and 1 Torr pressure in the DSC. The spectrum recorded in the absence of CCP plasma results from absorption by only NF_3 and NH_3 and can be reconstructed by adding absorbance spectra from 16 mT of NF_3 and 20 mT of NH_3, which indicates their partial pressures in the DSC. Striking a 350 W, CCP plasma results in and important diminution of the partial pressures of NF_3 and NH_3, which are highly dissociated by the discharge, and hence in weaker absorbance. The new absorption spectra with the CCP plasma ON can be reconstructed by adding absorbance spectra of 7.7 mT of NF_3, 4 mT of NH_3 and 20 mT of HF. Thus about 50% of NF_3 and 80% of NH_3 of the introduced gas have been dissociated by the plasma and, as will be discussed in following sections, the chain reactions of the dissociation products lead to the formation of HF molecules.

The partial pressures of NF_3, NH_3 and HF in all gas mixtures and plasma conditions have been deduced following the same procedure than in Fig. 6, by the best adjustment of the recorded absorption spectrum with the sum of three absorbance curves of these molecules with adequate amplitudes. Considering the reproducibility of results from several experiments, the uncertainty on determined partial pressures is estimated to be about 7% of the evaluated values + 1 mTorr.

3.2 Kinetics of NF_3/H_2 plasmas

Dissociation of NF_3 in the CCP plasma produces also NF_2 and NF radicals that rapidly react with H atoms, produced by the dissociation of H_2 in the CCP, but also reaction (2). The chain reactions which follow are:

$$H + NF_2 \rightarrow NF + HF \quad (9)$$

$$H + NF \rightarrow N + HF \quad (10)$$

$$NF + NF \rightarrow N_2 + 2\,F \quad (11)$$

for which the rate coefficients reported in the literature are: k_9=1.9 x 10^{-17} $m^3.s^{-1}$ [50]; k_{10}=2.5 x 10^{-17} $m^3.s^{-1}$ [50, 51] and k_{11}=7 x 10^{-17} $m^3.s^{-1}$ [50,51]. These fast chain reactions, whose main final product is HF molecule, can continue as far there are enough H_2 molecules and/or CCP generated F atoms in the chamber. Figure 7 illustrates the consumption of plasma generated F atoms and production of HF in NF_3/ H_2/ He (100/100/1900 sccm) gas mixture and pressure fixed at 1 Torr in the *DSC*. With increasing RF power of the CCP, the steady-state partial pressure of NF_3 in the downstream chamber drops gradually from its initial value of 52 mTorr to 20 mTorr at 350 W. Simultaneously, the partial pressure of produced HF molecule increases, reaching 90 mTorr at 350 W. It is also shown in this figure the ratio between the partial pressure of HF and the missing partial pressure of NF_3. This ratio clearly shows that three HF molecules are produced for one missing NF_3 molecule, indicating that once a NF_3 molecule starts to be dissociated, producing the first F atom, the chain reactions (2 and 9 to 11) will consume the other by-products of the dissociation (NF_2 and NF) to form HF molecules. In the above presented example, the limiting factor of the chain reactions is the amount of the plasma dissociated NF_3 molecules, which depends on RF power. Higher is the RF power, larger is the dissociation rate of NF_3 and larger is the amount of produced HF. However, the limiting factor can also be the amount of H atoms, produced by the plasma dissociation of H_2 molecules or by the reaction (2), available for the chain reactions. In figure 8 are reported the partial pressures of NF_3 and HF in the DSC versus the amount of H_2 in the feed gas, composed of 100 sccm of NF_3, *x* sccm of H_2 and 1900-*x* sccm of helium. The RF power in the CCP is fixed at 250 W and the total pressure in

the DSC is 1 Torr. At the beginning, with increasing H_2 flow rate, the partial pressure of HF increases almost linearly to reach its maximum at about 100 sccm of H_2, while NF_3 density remains almost constant. In fact, the dissociation rate of NF_3, thus the amount of F atoms in the DSC is fixed by the RF power in the CCP and up to 100 sccm of H_2 the total number of F atoms resulting from the dissociation of NF_3 exceeds the double of the number of introduced H_2 molecules. Thus, every H_2 of the feed gas produces two HF molecules. This is seen from the linear increase of the ratio (HF/dissociated NF_3) during the initial phase of the H_2 flow rate rise, also shown in figure 8. The actinometric emission intensity of the 703.7 nm F line in the auxiliary plasma, which is indicative of the partial pressure of fluorine atoms in the DSC, is also plotted in Fig. 8. Its behaviour indicates that, as expected, the density of F atoms in the DSC decreases as the H_2 flow rate increases up to about 100 sccm. Above this value, there are enough H_2 molecules in the reactor to consume all F atoms of the dissociated NF_3 molecules, and the intensity of the 703.7 fluorine line from the auxiliary plasma remains zero.

In conclusion, below 100 sccm of H_2, this is the amount of H_2 molecules of the feed gas which limits the quantity of HF produced inside the reactor but above 100 sccm, the dissociation rate of NF_3 will become the limiting factor. However, as the amount of H_2 in the feed gas becomes significant, its vibrational and rotational excitation will lead to a slight lowering of the electron temperature in the CCP plasma, resulting in a small diminution of the dissociation rate of NF_3. This is the reason for the small enhancement of the partial pressure of NF_3 after its minimum density at 100 sccm of H_2 and the simultaneous lowering of the HF density, as seen in Fig. 8. However, the ratio of the partial pressures of HF over the dissociated NF_3 remains close to 3, attesting that any of NF_3 molecules that starts to be dissociated by losing a flour atom, is fully consumed by the chain reactions (2 and 9 to 11) to form, in the end, three HF molecules.

3.3 Kinetics of NF_3/ NH_3 plasmas

F and H atoms produced in the CCP chamber by the dissociation of NF_3 and NH_3, trigger a series of chain reactions which leads to the production of large amount of HF molecule. In table 1 are reported the measured partial pressures of NF_3, NH_3 and HF in the gas introduced into the reactor chamber (plasma off, 0 W) and for 3 different RF powers. The introduced gas mixture is

NF_3/ NH_3/ He (50/50/1950 sccm) and the pressure in the *DSC* is fixed to 1 Torr. In the absence of plasma, the partial pressures of NF_3 and NH_3 are 25 and 27 mTorr, respectively. Striking the CCP plasma in the upper chamber with 150 W RF power, results in a drastic decrease (by factor 7) of the NH_3 partial pressure in the down-stream chamber whereas that of NF_3 is only divided by 2. This different behaviour is opposite to an expectation based on binding energy of F atom in NF_3 (2.9 eV) and H atom in NH_3 (4.1 eV), which should favour a higher dissociation rate of the former. But the difference reflects the fact that electron impact is the only process responsible for the dissociation of NF_3 molecules whereas the so produced F atoms can also react with NH_3, according to the reactions (4) and (12) [52, 53, 54, 15]:

$$HF + NH_3 \rightarrow NH_4F \qquad (12)$$

Reaction (4), which is very fast with k_4= 1-4 x10^{-16} $m^{-3}.s^{-1}$ according to the temperature [30], can explain why the newly generated HF molecule, with its partial pressure of 28 mTorr, becomes the most abundant molecule in the *DSC* at the lowest 150 W of CCP power

RF Power (W)	Measured NF_3 (mT)	Measured NH_3 (mT)	Measured HF (mT)	Dissociated NF_3 (mT)	HF/missing NF_3	Dissociated NH_3 (mT)	HF/missing NH_3
0	25	27	0	0		0	
150	12	4	28	13	2,2	23	1,2
250	10	3	44	15	2,9	24	1,8
350	9	1,5	48	16	3,0	25,5	1,9

Table 1- Measured partial pressures of NF_3, NH_3 and HF at different RF power of CCP, together with dissociated parts of NF_3 and NH_3 and the ratios of HF over dissociated parts.

With increasing RF power, thus increasing plasma density in the CCP chamber, NF_3 and NH_3 are more dissociated but the enhancement of their dissociated parts, also reported in columns 5 and 7 of table 1, is much slowed down. Accordingly, the amount of the produced HF increases, but it seems to levels off above 300 W RF power. We note that when RF power exceeds 150 W, due to the excess of plasma generated H atoms, all F atoms produced by the dissociation of NF_3 are converted to HF molecule.

Figure 9 shows the impact of the NH_3 dilution (for a fixed NF_3 flow rate of 50 sccm and total flow rate of 2050 sccm at 250 W CCP power) on the densities of NH_3, NF_3, HF and also on the amount of NH_3 lost (compared to the plasma OFF). The variation of F is not shown because it drops rapidly below the detection limit as soon as 25 sccm of NH_3 is added to NF_3. The density of NF_3, whose gas flow rate is constant at 50 sccm, is increasing slowly with the amount of NH_3 injected in the discharge. This is attributed to the small decay of the electron temperature/density with increasing NH_3 density in the mixture. However, these variations remain small for NH_3 flow rate above 75 scmm: the amount of NF_3 loss (i.e. dissociated to produce F atoms) is almost constant in the range of 100 to 400 sccm NH_3 flow rate. The density of HF rises rapidly to reach a maximum value at 50 sccm NH_3, while at the same time the NH_3 density remains negligibly low. This behaviour is in good agreement with the results of Table 1 and with reaction (4): F atoms produced from NF_3 dissociation reacts rapidly with NH_3 to produce HF. As far there is enough F available, all the injected NH_3 molecules are consumed by reaction (4) and the HF density rise accordingly. The NH_3 is fully dissociated for its flow up to approximately 50 sccm, at which point there is no more F atoms available: the NH_3 density then increase and above 75 sccm it rises almost linearly with the NH_3 flow rate. Surprisingly the HF density appears to decay significantly when the NH_3 flow rate overpass about 50 sccm : once all F atoms available are consumed by NH_3 to form HF, one would expect the HF density to reach a steady state. Furthermore, the amount of NH_3 lost would also be expected to be constant for the same reason, although it shows a significant increase with the NH_3 flow rate. As a matter of fact, there seems to be a correlation between the amount of NH_3 lost and the amount of HF decreases after its maximum at 50 sccm of NH_3 when its flow rate increases above 75 sccm. This is strongly suggesting that reaction 12 is taking place efficiently under our conditions, i.e. that NH_3 reacts with HF to produce NH_4F, the main precursor for the formation of salts on the wafer. The NH_4F density can then be roughly estimated from the loss of HF or from the loss of NH_3, as shown in Figure 10. There is a relatively good agreement between the two estimations, although a significant divergence is observed at high NH_3 dilution where the NH_4F density deduced from NH_3 loss is significantly larger than that deduced from HF decrease. This is probably due to the assumption that the NH_3 loss is caused solely by reactions with HF: the NH_3 density is actually driven by several processes including for example the recombination $NH_2+H \rightarrow NH_3$ which depend on the H density and thus on the H recombination rate on the reactor walls to form H_2

(which may be plasma chemistry dependent). Nevertheless, our results show that significant amount of NH_4F is produced in the discharge at large NH_3 dilutions, i.e. the processing conditions used to form salts selectively on the oxydized silicon or nitride surfaces.

3.4 conclusions

The chemistry of downstream plasmas used for isotropic etching of Si alloys is investigated by VUV absorption spectroscopy and OES both in NF_3/H_2 and NF_3/NH_3 chemistries. In both cases VUVAS indicate the formation of large amounts of HF molecules which are expected to play a role in oxide etching. F atoms are shown to react rapidly with H_2 and NH_3 to produce HF until all the fluorine is consumed. H also react rapidly with NF_2 and NF, producing HF and consuming NF_x radicals, which couldn't be detected by UVAS in the downstream chamber. In the NF_3/NH_3 chemistry, the HF density is shown to decrease when the NH_3 flow rate is increased above the NF_3 flow rate. This decay scales with the amount of NH_3 that is lost, which is attributed to an efficient reaction between NH_3 and HF to form the NH_4F molecule that is supposed to be the precursor for salt formation on the wafer. The NH_4F density could be estimated based on the quantity of HF an NH_3 lost and the high NH_3 dilution that is required to etch selectively oxidized material correspond to the largest values of the ratio NH_4F/HF.

ACKNOWLEDGMENTS

This work was partly supported by LabEx Minos (No. ANR-10-LABX-55-01) and by the French RENATECH network. The authors would like to acknowledge Applied Materials for their technical support.

Figure Caption

Fig.1: Schematic of the experimental set up showing the downstream chamber with the small deported plasma (used for OES).

Fig.2: Top view of the reactor showing the VUVAS experiment with the D2 light source and the VUV monochrmator equipped with the CCD camera.

Fig.3: VUV absorption spectrum of NH_3 gas (no plasma) at several reactor filling pressures.

Fig.4: VUV absorption spectrum of NF_3 gas (no plasma) at several reactor filling pressures.

Fig.5 : Black cross (+): absorption spectra recorded in a the NF_3 (4%)/H_2 (9%)/He gas and adjusted with a pure NF_3 spectrum recorded at 40 mTorr (cyan line). Black open cirle (◦): Absorption spectrum recorded with the plasma ON (250 W). This spectrum can be fitted in its high wavelength part by the green curve, which correspond to NF_3 gas at 24 mTorr. By subtracting this NF_3 contribution to the overall spectrum, we obtain the VUV absorption spectrum of HF molecules (blue line), corresponding to a pressure of 40 mTorr HF according to its absorption cross section.

Fig.6: Black aster (): absorption spectra recorded in a NF_3/NH_3/He gas mixture gas/He gas and adjusted (green line) with the spectra from the abaques withe the sum of 16 mtorr of NF_3 and 20 mTorr of NH_3. Black open circle: Absorption spectrum recorded with the plasma ON (250 W). This spectrum can be fitted by the sum of three spectra: HF (20 mTorr), NF_3 (7.7mTorr) and NH_3 (4 mTorr)

Fig. 7 variations of the densities of HF and NF_3 as a function of the RF power in NF_3/H_2 plasmas. The hollow black squares show the ratio of the HF density divided by the density of NF_3 which is lost when the plasma is ON, indicating that each NF_3 lost leads to the formation of 3 HF molecules.

Fig. 8 : impact of the H_2 dilution in NF_3 on the densities of NF_3, HF, F and on the ratio of produced HF per NF_3 lost

Fig.9: Impact of the NH_3 flow rate in NF_3 (50 sccm flow rate) on the densities of NF_3, NH_3, HF and on the amount of NH_3 lost when the plasma is ON with 250 W RF power.

Fig.10: variation of the HF density as a function of the NH_3 dilution in the NF_3(50sccm)/NH_3 plasma. The magenta and green curves indicate the density of NH_4F deduced respectively from the loss of HF and from the loss of NH3 (assuming that NH_3 reacts with HF to form NH_4F)

Fig. 1

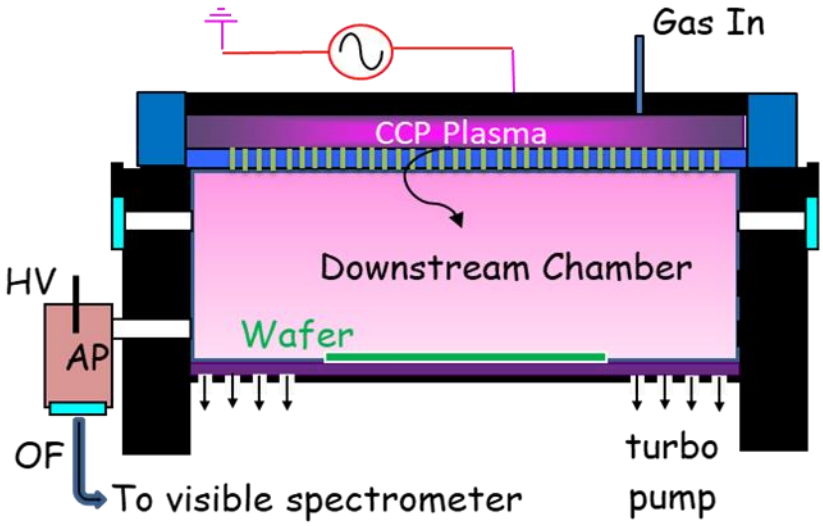
Gas In
CCP Plasma
Downstream Chamber
HV
AP
Wafer
OF
To visible spectrometer
turbo
pump

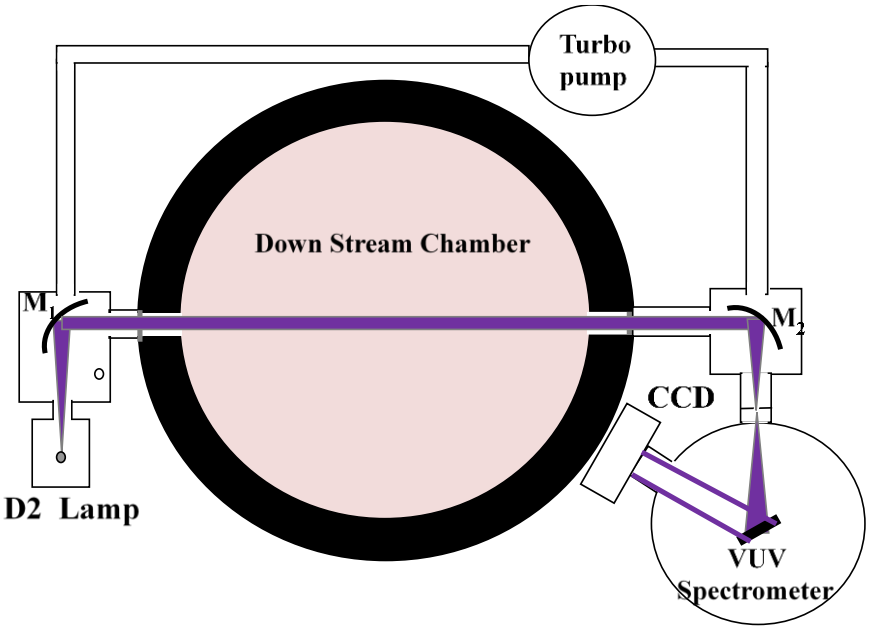
Turbo
pump
Down Stream Chamber
M1
M2
CCD
D2 Lamp
VUV
Spectrometer

Fig.2

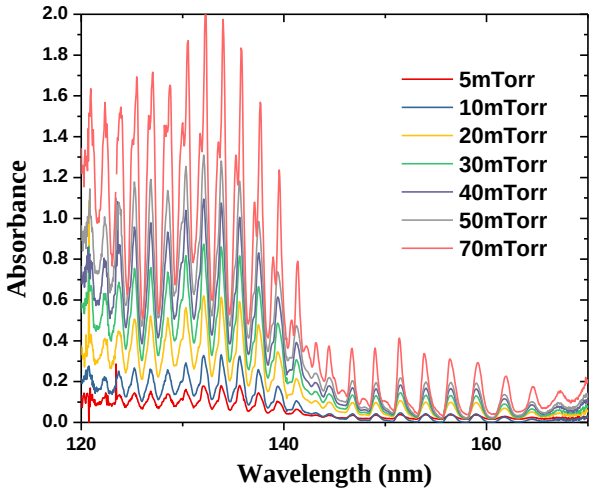
Absorbance
Wavelength (nm)
5mTorr
10mTorr
20mTorr
30mTorr
40mTorr
50mTorr
70mTorr
2.0
1.8
1.6
1.4
1.2
1.0
0.8
0.6
0.4
0.2
0.0
120
140
160

Fig. 3

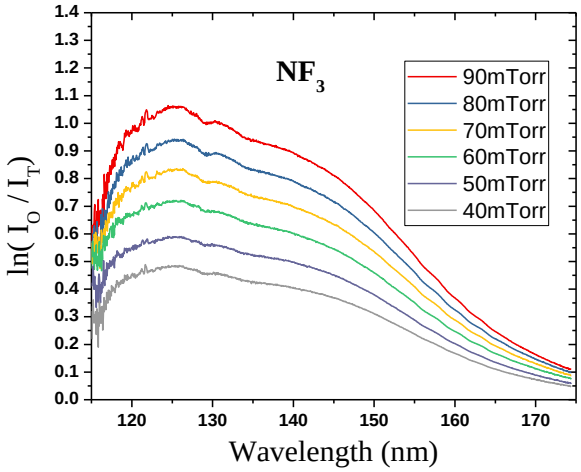
NF3
90mTorr
80mTorr
70mTorr
60mTorr
50mTorr
40mTorr
ln(I_O / I_T)
Wavelength (nm)
1.4
1.3
1.2
1.1
1.0
0.9
0.8
0.7
0.6
0.5
0.4
0.3
0.2
0.1
0.0
120
130
140
150
160
170

Fig.4

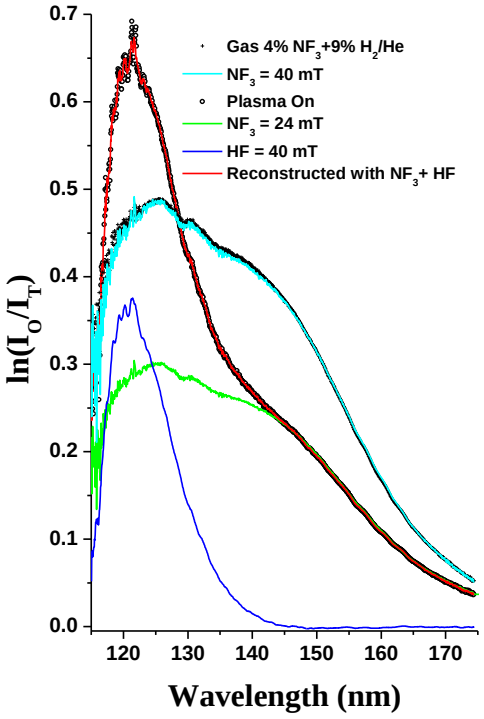
Gas 4% NF3+9% H2/He
NF3 = 40 mT
Plasma On
NF3 = 24 mT
HF = 40 mT
Reconstructed with NF3+ HF
ln(IO/IT)
Wavelength (nm)
0.0
0.1
0.2
0.3
0.4
0.5
0.6
0.7
120
130
140
150
160
170

Fig.5

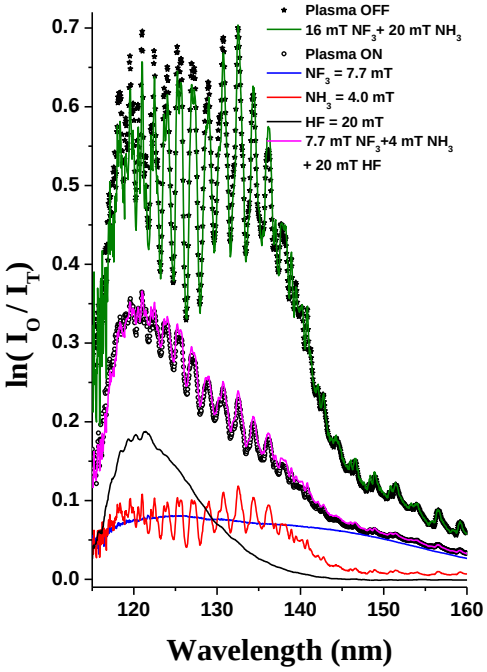
Plasma OFF
16 mT NF3+ 20 mT NH3
Plasma ON
NF3 = 7.7 mT
NH3 = 4.0 mT
HF = 20 mT
7.7 mT NF3+4 mT NH3
+ 20 mT HF
ln(I0 / IT)
Wavelength (nm)
0.0
0.1
0.2
0.3
0.4
0.5
0.6
0.7
120
130
140
150
160

Fig. 6.

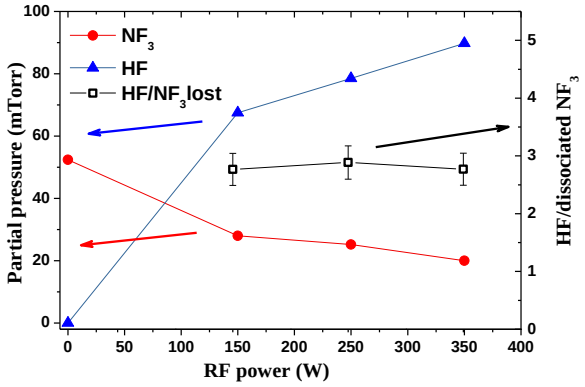
NF3
HF
HF/NF3 lost
Partial pressure (mTorr)
HF/dissociated NF3
RF power (W)
0
20
40
60
80
100
0
1
2
3
4
5
0
50
100
150
200
250
300
350
400

.

Fig. 7

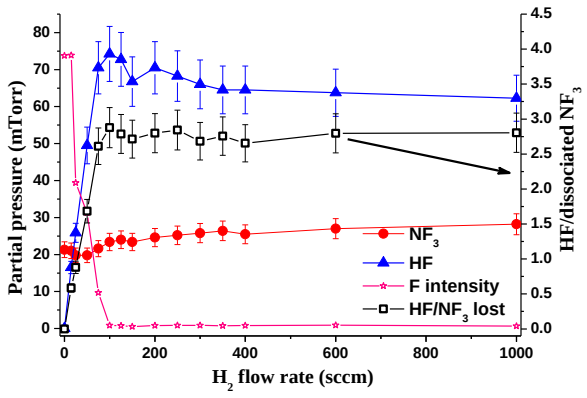
Partial pressure (mTorr)
HF/dissociated NF3
H2 flow rate (sccm)
NF3
HF
F intensity
HF/NF3 lost
0
10
20
30
40
50
60
70
80
0.0
0.5
1.0
1.5
2.0
2.5
3.0
3.5
4.0
4.5
0
200
400
600
800
1000

Fig. 8

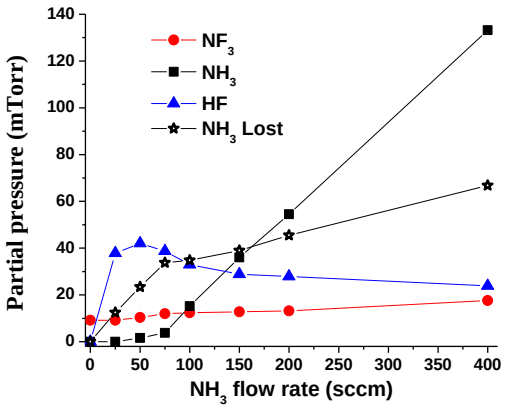
Partial pressure (mTorr)
NH3 flow rate (sccm)
NF3
NH3
HF
NH3 Lost
0
20
40
60
80
100
120
140
0
50
100
150
200
250
300
350
400

Fig. 9.

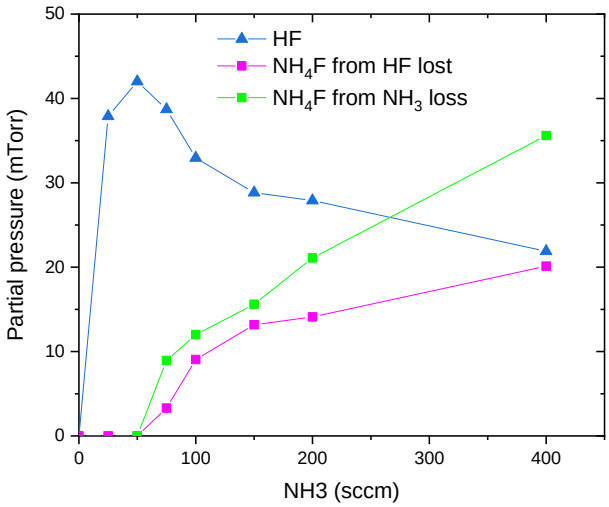
HF
NH4F from HF lost
NH4F from NH3 loss
Partial pressure (mTorr)
NH3 (sccm)
0
10
20
30
40
50
0
100
200
300
400

Fig. 10.

[1] S. M. Irving, Solid State Technol. 1971 **14**, 47

[2] V. M. Donnelly and A. Kornblit, J. Vac. Sci. Technol. 2013, **A 31**, 050825-1

[3] C. T. Carver, J. J. Plombon, P. E. Romero, S. Suri and Z. Tristan A. Tronic, and R. B. Turkot, Jr. 2015, *ECS Journal of Solid State Science and Technology*, **4** (6) N5005-N5009

[4] J. Jang et al. 2009, IEEE Symposium on VLSI Technology **p**. 192

[5] E. Prévost, G. Cunge, C. De-Buttet, S. Lagrasta, L. Vallier, C. Petit-Etienne, 2017, Proc. of SPIE Vol. 10149, 101490M,

[6] N. Posseme, O. Pollet, and S. Barnola 2014, Appl. Phys. Lett. **105**, 051605

[7] E-J Song, J-H. Kim, J-D. Kwon, S-H. Kwon, and J-H. Ahn 2018, Japanese Journal of Applied Physics **57**, 106505

[8] S. Huang, V. Volynets, J. R. Hamilton, S-Ki Nam, I-C. Song, S. Lu, J. Tennyson, and M. J. Kushner 2018, Journal of Vacuum Science & Technology A: Vacuum, Surfaces, and Films **36**, 021305

[9] B. E. E. Kastenmeier, P. J. Matsuo, G. S. Oehrlein, and J. G. Langan 1998, J. Vac. Sci. Technol., **A 16**, 2047

[10] H. Nishino, N. Hayasaka, and H. Okano 1993, J. Appl. Phys. **74**, 1345

[11] M. T. Suzuki, J. Kikuchi, M. Nagasaka, and S. Fujimura 1997, Mat. Res. Soc. Symp. Proc. Vol. 477

[12] W.S. Kim, W.G. Hwang, I.K. Kim. K.Y. Yun, K.M. Lee, and S.K. Chae 2005, Solid State Phenomena, **103**, 63

[13] Y. Hagimoto, H. Ugajin, D. Miyakoshi, H. Iwamoto, Y. Muraki, and T. Orii 2008, Solid State Phenomena, **134**, 7

[14] T. Kusuki, H. Kawakami, H. Sakaue and Y. Horiike 1993: Ext. Abstr. Electrochem. Soc. Meet., Hawaii, p. 375

[15] H. OGAWA, T. ARAI, M. YANAGISAWA, T. ICHIKI and Y. HORIIKE 2002, Jpn. J. Appl. Phys. **41** , 5349

[16] A. J. Sidhwa, F. C. Goh, H. A. Naseem, and W. D, Brown 1993, J. Vac. Sci. Techno!. **A 11**, 1156

[17] K. Shinoda, N. M., H. Kobayashi, M. Izawa, T. Saeki, K. Ishikawa, and M. Hori 2019, Journal of Vacuum Science & Technology **A 37**, 051002

[18] V. Martirosyan, E. Despiau-Pujo, J. Dubois, G. Cunge, and O. Joubert 2018, J. Vac. Sci. Technol. **A 36**, 041301

[19] V. Martirosyan, O. Joubert , E. Despiau-Pujo 2018, Journal of Physics D; Applied Physics **52**, 055204

[20] V. Ah-Leung, O. Pollet, N. Possémé, M. Garcia, B. Névine Rochat, C. Guedj, G. Audoit, and S. Barnola 2017; Journal of Vacuum Science & Technology A: Vacuum, Surfaces, and Films **35**, 021408

[21] N. Posseme, V. Ah-Leung, O. Pollet, C. Arvet and M. Garcia-Barros 2016, J. Vac. Sci. Technol. A **34**, 061301

[22] V. Renaud, C. Petit-Etienne, J-P. Barnes, J. Bisserier, O. Joubert, and E. Pargon 2019, J. Appl. Phys. **126**, 243301

[23] A. Tavernier, L. Favennec, T. Chevolleau, and V. Jousseaume 2012, ECS Trans. **45**, 225

[24] H. J. Oh, J. H. Lee, M. S. Lee, W. G. Shin, S. Y. Kang, G. D. Kim, and D. H. Ko 2014, ECS Trans. **61**, 1

[25] M. A. A.Clyne, D. J. McKenney and R. F. Walker, 1973, Can. J. Chem., **51**, 3596

[26] R. F. Heidner, J. F. Bott, C. E. Gardner and J. E. Melzer, 1979, J. Chem. Phys., **70**, 4509

[27] K. H. Homann, W. C. Solomon, J. Warnatz, H. Gg. Wagner, and C. Zetzsch 1970, Ber. Bunsenges. physik. Chemic **74**. 585

[28] E. Wurzburg, and P. L. Houston, 1980, J. Chem. Phys., **72**, 4811

[29] J.M.Herbelin and N. Cohen1973, Chemical Physics Letters, **20**, 605

[30] L. Tian, Y. Zhu, and H. Song and M. Yang, 2019. Phys. Chem. Chem. Phys., **21**, 11385

[31] G Cunge, M Fouchier, M Brihoum, P Bodart, M Touzeau, and N.sadeghi 2011. *Journal of Physics D: Applied Physics*, **44**, 122001

[32] G. Cunge, P. Bodart, M. Brihoum, F. Boulard, T. Chevolleau, and N. Sadeghi 2012, *Plasma Sources Science and Technology*, **21**, 4006

[33] J. W. Coburn, and H. F. Winters 1979, J. Vac. Sci. Technol. **16** , 391

[34] V. M. Donnelly and M.J. Schabel, 2002, J. Appl. Phys. **91**, 6288

[35] J-P. Booth, O. Joubert, J. Pelletier and N. Sadeghi 1991, J. Appl. Phys. **69**, 618

[36] J-P. Booth, and N. Sadeghi 1991, J. Appl. Phys. **70**, 611

[37] J-P. Booth, G. Cunge, F. Neuilly and N. Sadeghi 1998 Plasma Sources Sci. Technol. **7** 423

[38] Kogelschatz M, Cunge G and Sadeghi N 2004 J. Phys. D: Appl. Phys. **37** 1954

[39] Cunge G, Fouchier M, Brihoum M, Bodart P, Touzeau M. and Sadeghi N 2011 J. Phys. D: Appl. Phys. **44** 122001

[40] B-M. Cheng *et al*, 2006 Astrophysical Journal **647** 1535

[41] J A. Syage, R B Cohen and J. Steadman 1992 J. Chem. Phys. **97** 6072

[42] V. Vaida, M I. McCarthy, P C. Engelking and P. Botschwina 1987 J. Chem. Phys. **86** 6669

[43] Wu *et al* 2007 J. Chem. Phys. **127** 154311

[44] S R. La Paglia and A B F. Duncan 1961 J. Chem. Phys. **34** 1003

[45] T. Shirafuji and K. Tachibana 1994 Applied Surface Science **79** 117

[46] V C. Papadimitriou, M R. McGillen, E L. Fleming, C H. Jackman and J B. Burkholder 2013 Geophys. Research Lett. **40** 440

[47] J B Nee, M. Suto and L C. Lee, 1985 J. Phys. B: At. Mol. Phys. **18**, L293

[48] F. Carnovale, R. Tseng and C E. Brion, 1981 J. Phys. B: At. Mol. Phys. **14**, 4771

[49] Huber K P and Herzberg G 1979 Molecular Spectra and Molecular Structure: Constants of Diatomic Molecules, vol IV (New York: van Nostrand-Reinhold)

[50] C T. Cheah, M A A. Clyne and F D. Whitefield, 1980, J. Chem. Soc. Faraday Trans. II, **76** 711

[51] C T. Cheah and M A A. Clyne 1981, J. Photochemistry **15** 21

[52] J J. Sloan, D.G. Watson and J. Williamson, Chem. Phys. Lett. **74** (1980) 481

[53] C. Xiao, G. Shen, X. Wang, H. Fan, and X. Yang, J. Phys. Chem. **114** (2010) 4520

[54] H. Nishino, N. Hayasaka and H. Okano, J. Appl. Phys. **74** (1993) 1345